Automatic landmarking as a convenient prerequisite for geometric morphometrics. Validation on cone beam computed tomography (CBCT)-based shape analysis of the nasal complex

AF Ridel[a],*, F Demeter[b,c] , M. Galland[c], EN L'abbé[a], D Vandermeulen[a,d], AC Oettlé[a,e]

[a] Department of Anatomy, Faculty of Health Sciences, University of Pretoria, Pretoria, South Africa

[b] Lundbeck Foundation GeoGenetics Centre, Globe Institute, University of Copenhagen, Copenhagen, Denmark

[c] Musée De l'Homme, UMR7206, 17 Place Du Trocadéro, 75116 Paris, France

[d] Center for Processing Speech and Images (PSI), Department of Electrical Engineering (ESAT), KU Leuven, Belgium

[e] Department of Anatomy, School of Medicine, Sefako Makgatho Health Sciences University, Ga-Rankuwa, Pretoria, South Africa

*****Corresponding author at: Tswelopele Building, University of Pretoria, Private Bag X323, Arcadia 0007, South Africa. Alison.ridel.up@gmail.com

Highlights

- Cone beam computed tomography (CBCT) scans of adult South Africans were selected.
- Manual and automatic landmarks registered on the hard- and soft-tissue of the nose.
- Measurement error, systematic error and relative random errors were quantified.
- Validation of the automatic landmarking on hard-and soft-tissue 3D surfaces.

Abstract

Manual landmarking is used in several manual and semi-automated prediction guidelines for approximation of the nose. The manual placement of landmarks may, however, render the analysis less repeatable due to observer subjectivity and, consequently, have an impact on the accuracy of the human facial approximation. In order to address this subjectivity and thereby improve facial approximations, we are developing an automated three-dimensional (3D) method based on an automatic dense landmarking procedure using non-rigid surface registration. The aim of this study was to validate the automatic landmarking method by comparing the intra-observer errors (INTRA-OE) and inter-observer errors (INTER-OE) between automatic and manual landmarking.

Cone beam computed tomography (CBCT) scans of adult South Africans were selected from the Oral and Dental Hospital, University of Pretoria, South Africa. In this study, the validation of the automatic landmarking was performed on 20 3D surfaces. INTRA-OE and INTER-OE

were analyzed by registering 41 craniometric landmarks from 10 hard-tissue surfaces and 21 capulometric landmarks from 10 soft-tissue surfaces of the same individuals. Absolute precision of the landmark positioning (both on the samples as well as the template) was assessed by calculating the measurement error (ME) for each landmark over different observers. Systematic error (bias) and relative random error (precision) was further quantified through repeated measures ANOVA (ANOVA-RM).

The analysis showed that the random component of the ME in landmark positioning between the automatic observations were on average on par with the manual observations, except for the soft-tissue landmarks where automatic landmarking showed lower ME compared to manual landmarking. No bias was observed within the craniometric landmarking methods, but some bias was observed for capulometric landmarking.

In conclusion, this research provides a first validation of the precision and accuracy of the automatic placement of landmarks on 3D hard- and soft-tissue surfaces and demonstrates its utilization as a convenient prerequisite for geometric morphometrics based shape analysis of the nasal complex.

Keywords

Non-rigid surface registration; Automatic craniometric landmarking; Automatic capulometric landmarking; Manual landmarking; Intra- and inter- observer errors

1. Introduction

Each year in the Gauteng province of South Africa, approximately 1300 unidentified bodies are incinerated [1]. It is not always possible to identify unknown persons with conventional methods by comparing DNA and fingerprints. Additionally, many poor South Africans do not have dental or hospital records, or identification documents. As a result, more creative methods, including craniofacial reconstruction (CFR), have been implemented to assist in the identification of unknown persons from their skeletal remains. Craniofacial reconstruction methods can be used to estimate the ante mortem appearance of an individual from skeletal remains, providing a presumptive identification of the individual, which can be conveyed to the public. Craniofacial reconstruction is based on the assumed morphological relationship between the soft- tissue envelope and the underlying skull substrate [2]. Traditional CFR methods are based on 2D or 3D manual reconstruction by physically modelling a face on a skull replica with clay or plasticine [[3], [4], [5], [6], [7], [8]]. In the literature, these traditional reconstructions have been commonly classified as “Russian”, “American” or “Combination” methods [9]. It was recognized by the scientific community in the field of CFR that manual reconstruction methods require a high degree of anatomical and sculptural expertise and, as a result, remain difficult and subjective [[10], [11], [12], [13], [14], [15]]. The interpretations of two different artists can result in the creation of two substantially different faces from the same skull [14]. Therefore, traditional manual techniques are unsuitable for application to the judicial system, which requires precision, reliability and knowledge of possible quantization [14].

Recent developments in digital imaging techniques have resulted in the collection of large databases of 3D representations of hard- and soft-tissues of the face. Researchers in the field of CFR utilize these sources of information to improve objectivity in the reconstruction process [2,[14], [15], [16], [17]]. In CFR, all computer-assisted methods share the foundational premise that information about the complete skull versus information of the skin is used for mapping a template face onto a dry skull [2,[14], [15], [16], [17]]. Recently, Schlager [2] and Guyomarc'h [15], developed computer-assisted methods for the prediction of the structure of the external surface of the nose based on conventional computer tomography (CT) scans. Compared with manual methods, automation of facial approximation offers increased objectivity and the possibility of standardization [15]. However, the use of conventional CT scans as initial references may be influenced by supination effects on the face due to the horizontal position of the patient during scanning [18]. Moreover, the slice thickness, which generally ranges from 0.6 mm to 1.5 mm [2,15], induces errors of at least the same order of magnitude in the manual landmark placement on the 3D hard- and soft-tissue surfaces.

Previously described methods for approximation of the nose involve manual placements of landmarks for the definition of the region of interest [2,15]. When analysing the results of these methods, it seems that some craniometric and capulometric landmark positions are prone to inter-and intra-observer errors such as the nasal depth [2], the external (1.6–2.3 mm) and superior alar curvature [2,15] (1.5–2.3 mm), the alare [2,15] (1.9–2.9 mm) [2,15] and the submaxillare curvature [15] (1.6–3.7 mm). Manual placement of landmarks is extremely time consuming on large 3D surface samples and may induce important observer subjectivity and errors [[19], [20], [21], [22], [23], [24]]. Errors in manual landmarking are determined by factors such as the inherent variability among individuals in the sample and the metric quality of the instruments used [[25], [26], [27], [28]]. As a result, manual landmarking may render the analysis less repeatable and accurate for the facial approximation process. In the field of craniofacial reconstruction, the scientific literature concerning the utilization of automatic landmarking on 3D surfaces for the approximation of facial features (e.g. nose, eyes, mouth and ears), or the complete face, is limited. Limited research has been published regarding facial recognition implications for 2D [[29], [30], [31], [32], [33]] and 3D [24,34] capulometric landmarks, whereas no research has been done on the automatic landmarking of craniometric and capulometric landmarks on hard- and soft-tissue 3D surfaces.

The main critiques of current facial approximation techniques are the inherent subjectivity in manual methods, the references used and the lack of standardization, which limit the accuracy of the estimation [[10], [11], [12], [13], [14], [15]]. In order to improve the accuracy of facial approximation, we are developing an automated three-dimensional (3D) method based on an automatic dense landmarking procedure. Moreover, instead of using conventional CT for the acquisition and extraction of the relevant anatomical structures, we used cone beam CT (CBCT). During a CBCT scan, the patient is in a vertical position and the scanner rotates around the head, capturing images using a cone-shaped X-ray beam. The advantages of CBCT compared to CT include lower radiation dose, lower cost and higher spatial resolution (0.1 mm to 0.4 mm) for the placement of 3D landmarks [35]. Furthermore, the patient's upright position during acquisition minimizes gravitational effects on soft-tissue deformations. The aim of this study was to evaluate the measurement error (ME) of

the automatic versus the manual landmarking method, defined as the difference between repeated measurements of the same variable made by the same (i.e., INTRA-OE) or different observers (i.e., INTER-OE) [36]. A further aim of this study was to demonstrate the utilization of automatic landmarking as a convenient prerequisite for geometric morphometrics, based on shape analysis of the nasal complex.

2. Materials & methods

Cone beam computer tomography scans of ten adult South Africans were selected from the Oral and Dental Hospital, University of Pretoria, South Africa. Cone beam computer tomography scans were obtained using a CBCT scanner (Planmeca ProMax ® 3D, Pretoria, South Africa) with the following properties: 90 kV, 11.2 mA, voxel size of 0.4 mm and field of view of 230 × 260 mm. In order to standardize the acquisition, the subjects were scanned in a seated position with their eyes closed and with a relaxed facial expression. Patients were excluded if they presented with any condition that could affect the morphology of the face (e.g. orthodontic treatment, pathological conditions, facial asymmetry, or any facial interventional reconstructive surgery). This research project was approved by the Main Research Ethics Committee of the Faculty of Health Sciences, University of Pretoria, South Africa (Ethics Reference No: 301/2016).

CBCT scans in DICOM format were imported into MeVisLab © v. 2.7.1 software to extract volume data and create 3D images. The segmentation (Fig. 2a) of different elements (hard- and soft-tissue) were obtained by finding the threshold values between segmented components according to the "Half Maximum Height" (HMH) quantitative iterative thresholding method [37]. Threshold values for hard-tissue varied between 1200–1250 and for the soft-tissue, between 400-450. In this study, the facial skeleton will be referred to as the hard-tissue, and the external structure of the nose as the soft-tissue.

Following facial approximation literature [2,15], and in order to conserve homology and comparability between studies, classic craniometric and capulometric landmarks (type I, II, and III [38] were used. INTRA-OE and INTER-OE were analyzed by registering craniometric landmarks from ten hard-tissue surfaces and capulometric landmarks from ten soft-tissue surfaces of the same individuals. A total of 62 landmarks, described in Table 1 and illustrated in Fig. 1 were used.

Table 1. Definition, abbreviation and nature of landmarks used [38].

	Landmarks	Abbreviation	Nature	Definition
Craniometric				
1	Nasion	n	Median	Intersection of the nasofrontal sutures in the median plane.
2	Mid-nasal	mn	Median	Midline point on the internasal suture midway between nasion and rhinion.
3	Rhinion	rhi	Median	Most rostral (end) point on the internasal suture. Cannot be determined accurately if nasal bones are broken distally.

	Landmarks	Abbreviation	Nature	Definition
4	Nasospinale	ns	Median	The point where a line drawn between the inferior most points of the nasal aperture crosses the median plane. Note that this point is not necessarily at the tip of the nasal spine.
5	Subspinale b	ss	Median	The deepest point seen in the profile view below the anterior nasal spine (orthodontic point A).
6	Akanthion	ak	Median	Most anterior midline point of the nasal spine.
7	Prosthion	pr	Median	Median point between the central incisors on the anterior most margin of the maxillary alveolar rim.
8/9	Zygotemporale superior	zts	Bilateral	Most superior point of the zygomatico-temporal suture.
10/11	Zygotemporale inferior	zti	Bilateral	Most inferior point of the zygomatico-temporal suture.
12/13	Jugale	ju	Bilateral	Vertex of the posterior zygomatic angle, between the vertical edge and horizontal part of the zygomatic arch.
14/15	Frontomalare temporale	fmt	Bilateral	Most lateral part of the zygomaticofrontal suture.
16/17	Frontomalare orbitale	fmo	Bilateral	Point on the orbital rim marked by the zygomaticofrontal suture.
18/19	Nasomaxillofrontale	nmf	Bilateral	Point at the intersection of the frontal, maxillary, and nasal bones.
20/21	Ectoconchion	ec	Bilateral	Lateral point on the orbit at a line that bisects the orbit transversely.
22/23	Orbitale	or	Bilateral	Most inferior point on the inferior orbital rim. Usually falls along the lateral half of the orbital margin.
24/25	Zygoorbitale	zo	Bilateral	Intersection of the orbital margin and the zygomaticomaxillary suture.
26/27	Maxillofrontale	mf	Bilateral	Intersection of the anterior lacrimal crest with the frontomaxillary suture.
28/29	Nasomaxillare	nm	Bilateral	Most inferior point of the nasomaxillary suture on the nasal aperture.
30/31	Alare	al	Bilateral	Instrumentally determined as the most lateral point on the nasal aperture in a transverse plan.
32/33	Piriform curvature	cp	Bilateral	Most infero-lateral point of the piriform aperture.
34/35	Nariale	na	Bilateral	Most inferior point of the piriform aperture.
36/37	Zygomaxillare	zm	Bilateral	Most inferior point onthe zygomaticomaxillary suture.
38/39	Submaxillare curvature	csm	Bilateral	Most supero-medial point on the maxillary inflexion between the zygomaxillare and the ectomolar.

	Landmarks	Abbreviation	Nature	Definition
40/41	Supra canine	sc	Bilateral	Point on the superior alveolar ridge superior to the crown of the maxillary canine.
Capulometric				
1	Pronasale	prn'	Median	The most anteriorly protruded point of the apex nasi.
2	Nasale inferius	ni'	Median	Most inferior point of the apex nasi.
3	Columella	c'	Median	Midpoint of the nasal columella crest, intersecting a line between the two cs' points.
4	Subnasale	sn'	Median	Median point at the junction between the lower border of the nasal septum and the philtrum area.
5/6	External alar curvature	eac	Bilateral	Most anterior point of the nasal wing at the maximum of curvature.
7/8	Superior alar curvature	sac	Bilateral	Most superior point of the nasal wing.
9/10	Alagenion	ag	Bilateral	Most posterior point of the nasal wing.
11/12	Alare	al'	Bilateral	The most lateral point on the nasal ala.
13/14	Alar curvature point	ac'	Bilateral	The most posterolateral point of the curvature of the base line of each nasal ala.
15/16	Mid-columella	mc'	Bilateral	Midpoint of the nasal columella crest on either side, where the columella thickness is measured (equivalent to Subnasale').
17/18	Nasal-depth	nd	Bilateral	Most medial point of the transition nose/eye.
19	Sellion	se'	Median	Deepest midline point of the nasofronal angle; not a substitute for n'.
20/21	Mid-nostril	mn	Bilateral	Midpoint of maximal nostril width - projected on the transition nostril/philtrum.

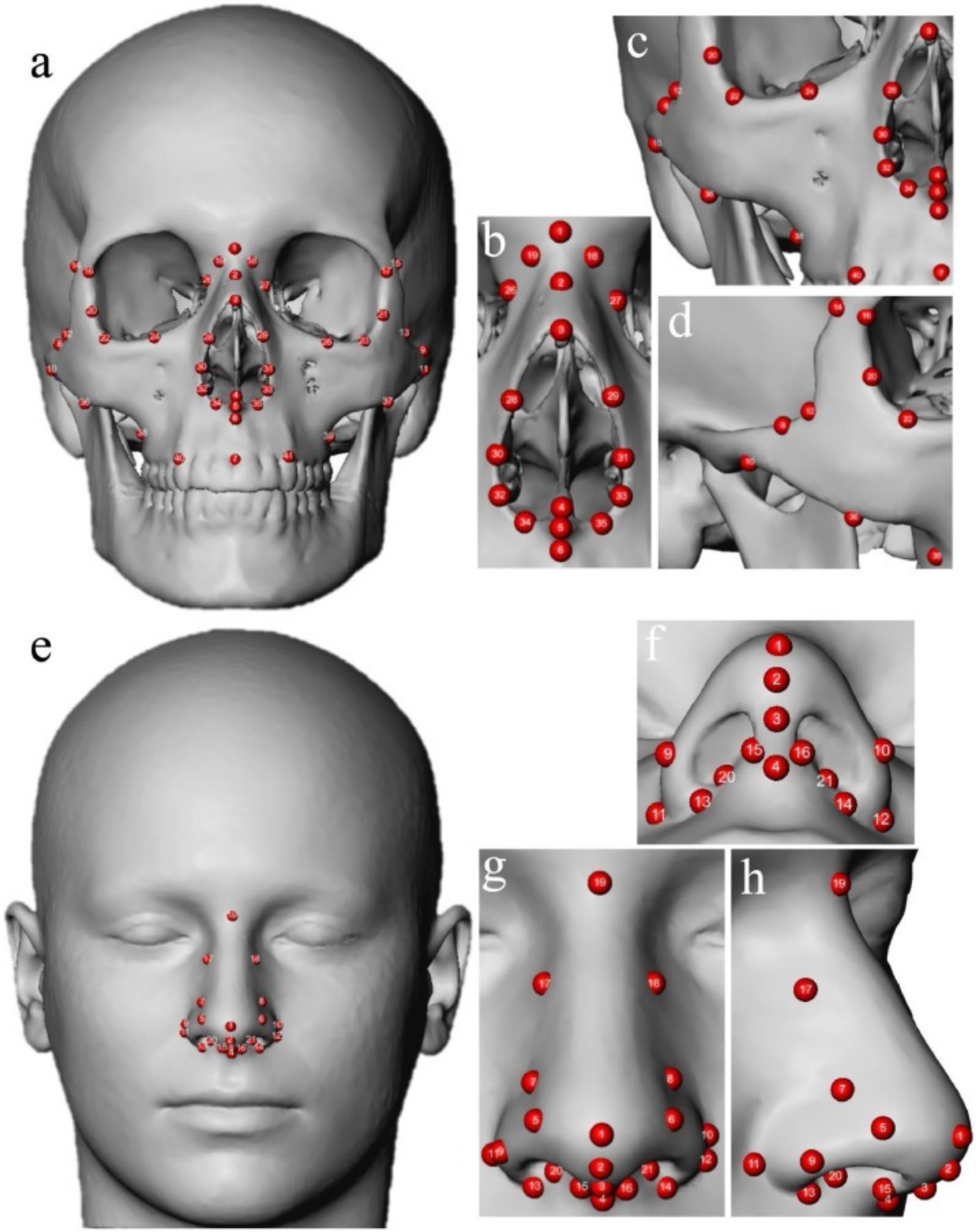

Fig. 1. Landmarks placed on the hard- and soft-tissue region of interest.

a: Frontal view of the hard-tissue region of interest; b: nasal superior and inferior; c: maxillary; d: zygomatic; e: frontal view of the soft-tissue region of interest; f: inferior view of the nose; g: anterior view of the nose; h: lateral view of the nose (cf. Table 1).

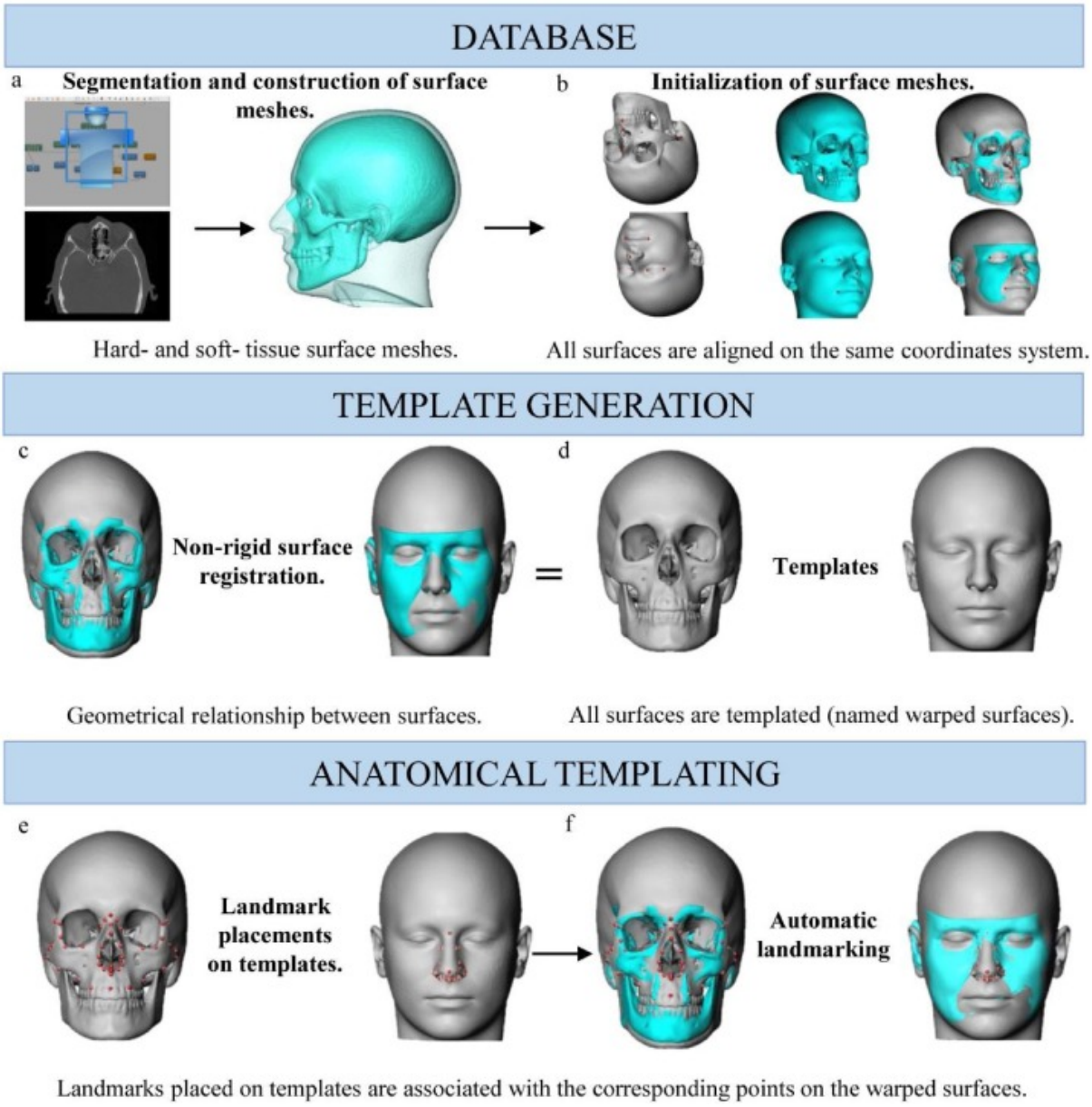

Fig. 2. Workflow of the automatic landmarking procedure. a) segmentation process; b) initialisation process; c) non-rigid surface registration process; d) templates generation; e) definition of the region of interest on templates; f) automatic landmarking.

Forty-one craniometric landmarks were recorded on the hard-tissue: 17 bilateral pairs and seven median landmarks. On the soft-tissue, 21 capulometric landmarks were recorded: eight bilateral pairs and five median landmarks. The landmarks selected were distributed on the facial skeleton and the external nose, creating a hard- and soft-tissue region of interest. The hard-tissue region of interest (Fig. 1a) was delimited by the facial skeleton comprising the nasal bones (Fig. 1b), the nasal aperture (Fig. 1b), the maxillae (Fig. 1c) and the zygomatic bones (Fig. 1d). The soft-tissue region of interest (Fig. 1e) was delimited by the surface anatomy as related to the hard-tissue, including mainly the external nose (Fig. 1g, h) and the nares (Fig. 1f).

2.1. Manual landmarking

The manual placement of landmarks was performed by indicating the 41 craniometric landmarks on the ten hard-tissue surfaces and the 21 capulometric landmarks on the ten soft-tissue surfaces. For the INTRA-OE, the manual placement of landmarks was performed twice by the same observer (noted AR1m and AR2m) on every subject, with an interval of two weeks. For the INTER-OE, the manual landmarking was performed twice by two different observers (noted AR1m and MGm). The manual placement was performed using MeVisLab software and the 3D coordinates of landmark points were recorded and saved in an Excel file for further analysis.

2.2. Automatic landmarking

The automatic landmarking method proposed here is adapted from the procedure introduced by Claes [39]. The basic concept involves a reference template of the anatomical surface of interest, containing a dense set of landmarks. These landmarks are a dense equivalent of traditional sparse, discrete, well-defined, anatomical landmarks. Reference hard- and soft-tissue templates (Fig. 2d) are created using a non-rigid- surfaces registration process (Fig. 2c). Prior to registration, all the surfaces are repositioned into the same coordinate system using an initialisation mesh procedure (Fig. 2b). The initialization is performed manually with indicating a set of landmarks on floating and target surfaces in order to interactively rotate and translate the surfaces so as to bring them into each other's proximity. These transformations map the coordinates of each point of the floating surface into the coordinate space of the target surface. The non-rigid surface registration results are dependent on the quality of this initial initialization procedure. Surface registration refers to the establishment of the geometrical relationship between surfaces that aligns the surfaces between them as well as possible. Then, every individual surface is "templated" (named the warped surfaces) such that every point on all 3D surfaces is associated with the anatomically corresponding point on the reference template. Therefore, information encoded in 3D-surface representations has to be extracted and made comparable. In a last step, landmarks are indicated once on the reference templates (Fig. 2e). Every landmark placed on the template is associated with the anatomically corresponding point on the warped surfaces.

During an anatomical templating process, the reference template is warped non-rigidly to every subject's anatomically corresponding surface (target surface). The non-rigid (robust) surface registration software used for this warping was developed using the MeVisLab © v. 2.7.1 software [40]. The warping is performed iteratively starting with a rigid alignment, and gradually following with more flexible registration steps. At the end of this process every landmark of the template is projected onto every subject's surface, thus establishing a dense point-based anatomical correspondence among all subjects (Fig. 2f). Therefore, the coordinates of all subjects are recorded within a common coordinate system which may be used for statistical analysis.

In order to estimate the precision/measurement error of this procedure, the discrete landmarks were twice indicated on the hard- and soft-tissue templates. The warped landmarks on the studied subjects were recorded (noted AR1a, AR2a, MGa). Note that the warping transformation remains the same, independent of the re-indication of the discrete

landmarks. For the INTRA-OE, the landmark indication on the templates was done by the same observer (noted AR1t, AR2t), with an interval of two weeks. For the INTER-OE, the landmark indication on the templates was done independently by two different observers (noted AR1t, MGt).

2.3. Statistical analysis

The raw coordinates resulting from the manual and automatic landmarking procedures were adjusted through a generalized Procrustes superimposition (GPS) to obtain pose-invariant shape coordinates [41,42]. More precisely, GPS reduces the sum of the squared distances between corresponding anatomical points by aligning the configurations of landmarks and removing the differences due to translation and rotation (not size) among all individuals thus defining the remaining shape information as a set of Procrustes coordinates [[43], [44], [45]]. We adapted the procedure to keep the relative position (and thus measurement error) of the samples of the same individual unchanged, while their common (per subject) mean is GPA aligned with the grand mean.

We distinguish between two types of measurement errors on landmark localization: precision and accuracy. Precision refers to the random error, in measuring the degree to which repeated measurements give the same result under the same conditions. In contrast, accuracy refers to the systematic error (or bias) of the measurements compared to their true values. Random error interferes with the genuine variability by adding residual noise and increases any Type II error rate (reduction in statistical power). In our particular setting ME reflects two different components of error: reproducibility due to different methods (automatic versus manual), which induces both systematic and random errors and repeatability due to multiple observers, which induces random errors. Since we do not have a ground truth available, we limit the assessment of the systematic error by evaluating the bias between the automatic and manual landmarking.

The precision of the (manual and automatic) landmark positioning was calculated using the dispersion Δ_{ij} for each landmark *i* and individual *j*. Dispersion is defined as the Mean Euclidean Distance (MED) of the sample landmark $\boldsymbol{p}_{ijk}$ to the mean $\overline{\boldsymbol{p}}_{ij}$ of the (x,y,z)-coordinates of landmark *i* over all observations *k* (INTER, INTRA, resp.) for subject *j*:

$$\Delta_{ij} = \sum_{k=1}^{K} \left|\left| \boldsymbol{p}_{ijk} - \overline{\boldsymbol{p}}_{ij} \right|\right| / K, \text{ with } \overline{\boldsymbol{p}}_{ij} = \sum_{k=1}^{K} \boldsymbol{p}_{ijk} / K$$

Boxplots of MED values are generated for automatic and manual landmarking separately, showing the variation of dispersion over different subjects. Global precision is then reported as the global (averaged over all landmarks) mean (μ_{Δ}) and median (m_{Δ}) of the per landmark mean ($\mu_{\Delta i}$) and median ($m_{\Delta i}$) values (over all subjects).

The precision of the manual landmarking was assessed by comparing the dispersion over the three observers (AR1m, AR2m, MGm) manually placing the landmarks on each subject. The precision of the automatic landmarking was calculated by indicating the craniometric and capulometric landmarks three times (AR1t, AR2t, MGt) on the templates and measuring the resulting dispersion on the automatically indicated landmarks (AR1a, AR2a, MGa) for

each subject. In addition, the precision of the landmark positioning on the templates was similarly calculated using MED on the three measurements (AR1t, AR2t, MGt).

While these absolute (expressed in metric units (mm)) measures are valuable in comparing the precision of different methods and possibly selecting a subset of landmarks to retain for further morphometric analysis, they should be supplemented by relative measures, comparing the ME to the true shape variation in the specific data sets.

The bias between automatic and manual landmarking was assessed both visually and statistically. Plotting the Procrustes shape measures (principal components) in the PCA tangent space along the first two principal components can reveal any structural grouping due to the methods. Bias was first examined by examining differences in mean shape of the landmark configurations obtained by the two (automatic and manual) methods, considered as independent populations.

Finally, both systematic (bias) and relative random error were assessed through a three-way repeated measures Procrustes ANOVA [[46], [47], [48]], with individual as a factor and with observer and method as additional factors. This procedure partitions the overall variation of Procrustes aligned landmark coordinates into separate components, allowing to evaluate the impact of variation due to methods (automatic versus manual) and observers (intra and inter) relative to true morphological variation between individuals. Intra-class correlation (also termed repeatability) was obtained using a one-way ANOVA with individual as unique categorical predicting variable [25,49].

All statistical analyses were performed using R studio software version 1.0.44-®2009-2016 for Windows [50].

3. Results

The global mean and median dispersion results are presented in Table 2, together with the dispersion of the three observations (AR1t, AR2t, MGt) of landmark positioning on the hard- and soft-tissue templates. While both mean and median dispersion are on par for automatic and manual craniometric landmarking (mean(median) values of 1.64 (1.64) mm vs 1.67 (1.63) mm), lower dispersion values were obtained for automatic compared to manual capulometric landmarking (1.31 (1.23) mm vs 1.66 (1.57) mm). The boxplots of the dispersion for automatic and manual craniometric and capulometric landmarking are shown in Fig. 3, Fig. 4. These plots show that the variation in dispersion in automatic landmarking is much smaller than in manual landmarking.

Table 2. Measurement errors (global mean and median dispersion in mm) for hard- and soft-tissue landmarks. Right column: mean dispersion for template landmarking.

	Automatic		Manual		Template
	Mean (mm)	**Median (mm)**	**Mean (mm)**	**Median (mm)**	**Mean (mm)**
Hard-tissue	1.64	1.64	1.67	1.63	1.63
Soft-tissue	1.31	1.23	1.66	1.57	1.26

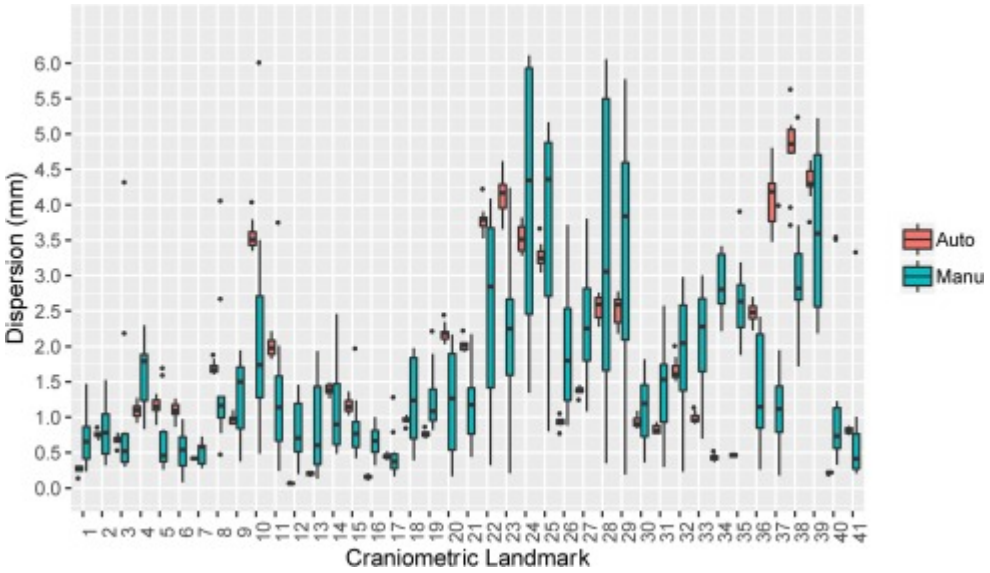

Fig. 3. Boxplots of the dispersion for automatic and manual craniometric landmarking. Craniometric landmark definitions (1–41): cf Table 1.

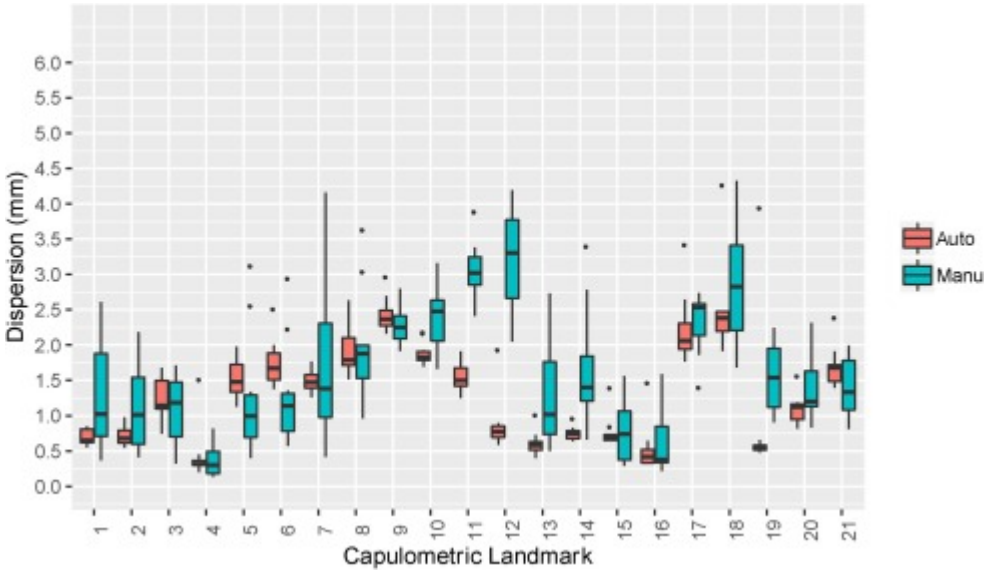

Fig. 4. Boxplots of the dispersion of automatic and manual capulometric landmarking. Capulometric landmark definitions (1–41): cf Table 1.

We also plotted the median dispersion per landmark of the automatic landmarking as a function of the median dispersion per landmark due to the multi-observer landmarking on

the templates for both the hard and the soft tissues (Fig. 5). We observe a strong linear correlation between both: automatic landmarking dispersion is almost exclusively determined by template landmarking dispersion, with little or no influence of inter-individual differences of the warping procedure.

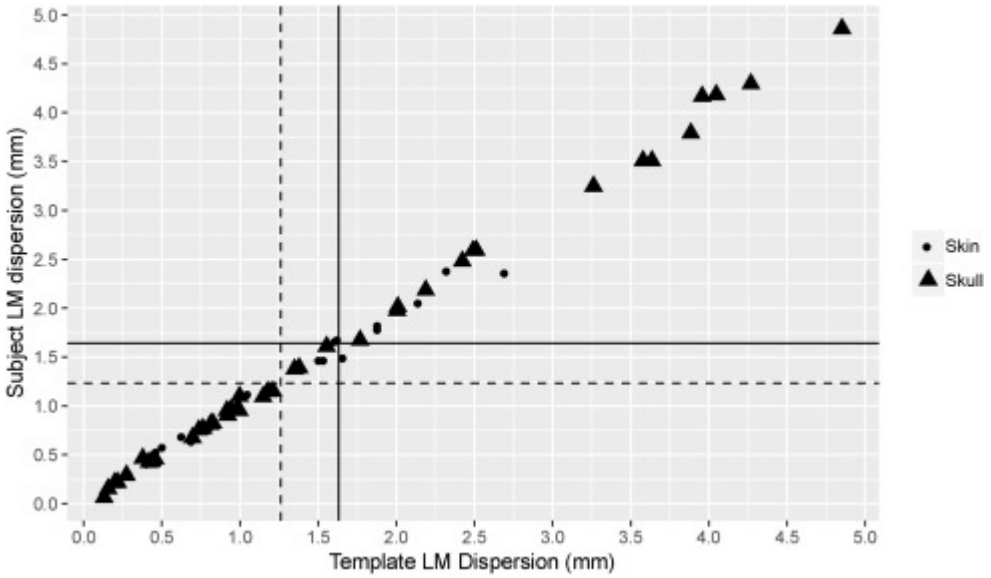

Fig. 5. Correlation between the dispersion (per landmark) on the automatically indicated landmarks and the dispersion on the corresponding landmarks on the templates. The solid (dashed) horizontal and vertical lines represent the global median dispersion for hard(skull) – and soft-(skin) landmarking (on target subjects and templates, respectively).

Fig. 6, Fig. 7 shows three different plots of the Procrustes aligned craniometric /capulometric coordinates projected onto the first two principal components in tangent space, grouped according to method and observer, method and individual. The graphs for the craniometric landmarking do not provide visual evidence of biases induced by observer and/or method. However, Fig. 7 indicate bias induced by method on the one hand (middle plot), and also observer, although mainly for the manual procedure (left plot).

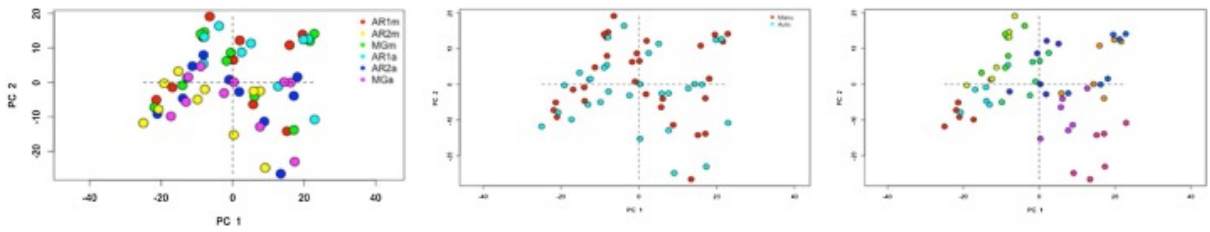

Fig. 6. Scatterplots of Procrustes craniometric shape coordinates (PC) onto the first two principal components. Left: colored according to method and observer, middle: colored according to method, right: colored according to individual.

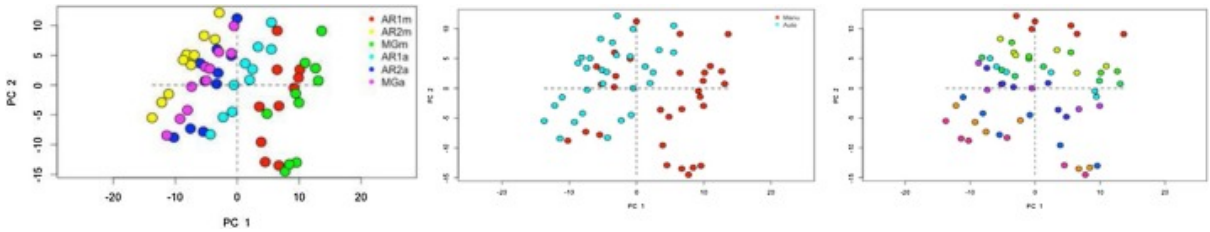

Fig. 7. Scatterplots of Procrustes capulometric shape coordinates (PC) onto the first two principal components. Left: colored according to method and observer, middle: colored according to method, right: colored according to individual.

The unpaired test of equal mean shapes for the automatic and manual landmark configurations returned p-values (according to different tests) lower than 0.01, indicating no significant differences in mean shapes due to the choice of method. The results of the 3-way Procrustes ANOVA are tabulated in Table 3 and in Table 4. From these tables we read that both method and observer have a statistically non-negligible contribution to total variance. However, the observer component for craniometric landmarking is far larger than the method component. This supports the conclusion that the automatic method has little influence on the ME for craniometric landmarking in line with the findings of Table 2 and Fig. 6.

Table 3. Three-way Procrustes ANOVA for capulometric landmarks.

	Df	SS	MS	Rsq	F	Z	Pr (>F)
Individual	9	4550.9	505.65	0.40100	10.7709	11.5281	0.001
Method	1	1566.2	1566.16	0.13800	33.3605	7.1559	0.001
Observer	2	2248.9	1124.46	0.19816	23.9519	9.4629	0.001
Method:Observer	2	870.2	435.12	0.07668	9.2684	10.6648	0.001
Residuals	45	2112.6	46.95	0.18615			
Total	59	11348.8					

Table 4. Three-way Procrustes ANOVA for craniometric landmarks.

	Df	SS	MS	Rsq	F	Z	Pr (>F)
Individual	9	22853	2539.2	0.56792	21.275	15.7904	0.001
Method	1	2259	2259.3	0.05614	18.929	7.4386	0.001
Observer	2	6587	3293.4	0.16369	27.593	11.0797	0.001
Method:Observer	2	3170	1585.1	0.07878	13.280	12.1300	0.001
Residuals	45	2112.6	46.95	0.18615			
Total	59	40 240					

For capulometric landmarking, however, the contribution of method attributed variance is larger, which corroborates the findings of Table 2, which indicates a lower dispersion for the automatic method and Fig. 7 (middle) which indicates a bias between automatic and manual landmarking. The inter- and intra- observer ME for both types of landmarks, on the other hand, contribute to a larger extent to total ME.

4. Discussion

The results obtained in this study validated the accuracy (bias) and the precision of the automatic placement of landmarks, both on hard- and soft-tissue surfaces. The automatic landmarking method allows us to reduce inter- and intra-observer errors and it could be a convenient prerequisite for geometric morphometrics as an alternative to manual landmarking. More generally, automatic landmarking offers many applications in forensic and physical anthropology using 3D surfaces.

The automatic placement of landmarks, in addition to reducing measurement errors in landmark placements, allows us to achieve a better precision for facial approximation, enabling the possibility to include more samples and populations with ease. Especially in CFR, when large sample sizes are required, manual placement of landmarks could be extremely time consuming and may be biased with observer subjectivity, rendering the analysis less repeatable and impacting on the precision of the human facial approximation. When we compare the results of our study to previous studies on the approximation of the nose using manual landmarking methods on 3D surfaces [2,15], it seems that the nasal depth and the superior alar curvature are prone to inter-and intra-observer errors. It could be due to the fact that the soft-tissue is very smooth and hence the interpretation of the curve's maximum, for instance, is quite ambiguous. The high random and standard errors noted in the automatic and manual placement of some craniometric landmarks (zygotemporal inferior, orbitale, zygoorbitale, nasomaxillare and submaxillare curvature) and capulometric landmarks (nasal depth and the superior alar curvature) could be problematic and precludes its use in the shape analysis of the nasal complex from 3D surfaces.

The results (both visually and statistically) show that the automatic procedure, as tested here, has similar, if not better, measurement error compared to the manual procedure. The resulting random component of ME is almost exclusively determined by the dispersion on the template landmarks. Random measurement error, in general, is known to be reduced by averaging the repeated measurements [25]. Hence, in order to further reduce this ME for automatic landmarking, one should obtain an average template landmark configuration either by averaging multiple indications on the template or defining a consensus configuration.

Extensive work has been published on 2D landmarks [[29], [30], [31], [32], [33]], whereas less research has been done on the identification and location of landmarks on 3D surfaces [24,34]. Only some recent work on 3D face registration explored the use of curvature in order to find the tip of the nose [[51], [52], [53]] in combination with an iterative closest point (ICP) alignment algorithm. The ICP is one of most popular techniques for 3D face registration and it has been extensively used as the main procedure, or in combination with

other methods [51,54,55]. Finally, we stress that this study is the first attempt at a computer-assisted facial approximation of the nose with an automatic landmarking approach for the South African population using CBCT scans.

Compared with manual methods, automation of facial approximation is suitable for application to the judicial system, which requires precision, reliability and knowledge of possible quantization errors. In addition, the automatic placement of landmarks on large 3D surface samples, offers the possibility of standardization and increased accuracy in the analysis of the correlations between hard- and soft-tissue facial features. In this research, we specifically used CBCT scans from living patients, since we intended to remove the limits generated by the use of dry skulls, cadavers and CT datasets as initial references, such as desiccation and supination effects. A further advantage of CBCT compared to CT includes higher spatial resolution (0.1 mm to 0.4 mm) and isotropic volumetric data for the accurate placement of 3D landmarks [35].

Finally, this research demonstrates the utilization of the automatic landmarking as a convenient prerequisite for geometric morphometrics-based shape analysis of the nasal complex. Future work using automatic landmarking for geometric morphometric purposed will have to concentrate on acquisition of larger databases. When planning future research, it will be fundamental to consider the integration of semi-landmarks as well, in order to describe and to visualize the structures more satisfactory, however, a much denser placement of coordinates would be required. The automatic landmarking needs to be applied on different 3D anatomical elements and on different populations before it can be considered robust. In addition, it would be interesting to test the precision of the automatic placement of landmarks on another facial skeleton element (for instance the mandible or forehead) and on external components of the face (for instance the mouth, eye, or ear), in order to finally apply the methodology on the complete skull/face. In general, when developing approaches using automatic landmarking, it may be useful to consider factors such as sex, age and inter-population morphological differences to possibly further enhance the accuracy of the methodology.

5. Conclusion

This research provides a validation of the precision of the automatic placement of landmarks and demonstrates its utilization as a convenient prerequisite for geometric morphometrics-based shape analysis of the nasal complex. The automatic landmarks positioning on hard- and soft-tissue 3D surfaces offers increased objectivity and the possibility of standardization. The automatic landmarking, in addition to reducing measurement errors, allows us to achieve a better precision for facial approximation, enabling the possibility to include more samples and populations with ease. Furthermore, the automatic placement of landmarks as an accurate alternative to manual landmarking, offers many applications in forensic and physical anthropology.

Acknowledgments

The authors would like to thank Dr. André Uys from the Oral and Dental Hospital, University of Pretoria, South Africa and Dr. Sarel Botha from the Life Groenkloof Hospital, Pretoria,

South Africa, for providing the CBCT-data. We acknowledge the AESOP + consortia coordinated by Prof. José Braga from the Computer-assisted Palaeoanthropology Team, UMR 5288 CNRS- Université Paul-Sabatier, 37, allées Jules-Guesde, 31000 Toulouse, and from the Evolutionary Studies Institute and School of Geosciences, University of the Witwatersrand, Johannesburg, South Africa, for the financial support.

References

[1] G.C. Krüger, L. Liebenberg, J. Myburgh, A. Meyer, A.C. Oettlé, D. Botha, D.M. Brits, M.W. Kenyhercz, K.E. Stull, C. Sutherland, E.N. L'Abbé, Forensic anthropology and the biological profile in South Africa, New Perspectives in Forensic Human Skeletal Identification, Elsevier, 2018, pp. 313–321, doi: http:// dx.doi.org/10.1016/B978-0-12-805429-1.00027-2.S.

[2] Schlager, Soft-tissue Reconstruction of the Human Nose: Population Differences and Sexual Dimorphism Doctoral dissertation, Universität, 2013.

[3] M.M. Gerasimov, Face Finder, CRC Press, NY, NY, 1971.

[4] G. Lebedinskaya, T. Balueva, E. Veselovskaya, Development of methodological principles for reconstruction of the face on the basis of skull material., in: M.Y. Işcan, R.P. Helmer (Eds.), Forensic Analysis of the Skull: Craniofacial Analysis, Reconstruction, and Identification, Wiley-Liss, New York, NY, 1993.

[5] C.C. Snow, B.P. Gatliff, K.R. McWilliams, Reconstruction of facial features from the skull: an evaluation of its usefulness in forensic anthropology, Am. J. Phys. Anthropol. 33 (1970) 221–227, doi: http://dx.doi.org/10.1002/ajpa.1330330207.

[6] J. Prag, R. Neave, Making Faces Using Forensic and Archeological Evidence, British Museum Press, London, 1997. [7] C. Wilkinson, Forensic Facial Reconstruction, Cambridge University Press, Cambridge, UK; New York, 2004.

[8] C. Wilkinson, Facial reconstruction – anatomical art or artistic anatomy? J. Anat. 216 (2010) 235–250, doi: http://dx.doi.org/10.1111/j.1469- 7580.2009.01182.x.

[9] C.N. Stephan, Beyond the sphere of the English facial approximation literature: ramifications of German papers on western method concepts, J. Forensic Sci. 51 (2006) 736–739, doi: http://dx.doi.org/10.1111/j.1556-4029.2006.00175.x.

[10] A.J. Tyrrell, M.P. Evison, A.T. Chamberlain, M.A. Green, Forensic three-dimensional facial reconstruction: historical review and contemporary developments, J. Forensic Sci. 42 (1997) 14176J, doi: http://dx.doi.org/ 10.1520/JFS14176J.

[11] C.N. Stephan, Anthropological facial 'reconstruction' – recognizing the fallacies, 'unembracing' the errors, and realizing method limits, Sci. Justice 43 (2003) 193–200, doi: http://dx.doi.org/10.1016/S1355-0306(03)71776-6.

[12] L. Verzé, History of Facial Reconstruction, 1, Vol. 80 (2009) pp. 5–12.

[13] H. Ullrich, C.N. Stephan, On Gerasimov's Plastic Facial Reconstruction Technique: New Insights to Facilitate Repeatability*: Gerasimov's plastic facial reconstruction techniques, J. Forensic Sci. 56 (2011) 470–474, doi: http:// dx.doi.org/10.1111/j.1556-4029.2010.01672.x

[14] D. Vandermeulen, P. Claes, S. De Greef, G. Willems, J. Clement, P. Suetens, Automated facial reconstruction, Craniofacial Identif. 203 (2012).

[15] P. Guyomarc'h, B. Dutailly, J. Charton, F. Santos, P. Desbarats, H. Coqueugniot, Anthropological facial approximation in three dimensions (AFA3D): computer-assisted estimation of the facial morphology using geometric morphometrics, J. Forensic Sci. 59 (2014) 1502–1516, doi: http://dx.doi.org/10.1111/ 1556-4029.12547.

[16] P. Claes, D. Vandermeulen, S. De Greef, G. Willems, J.G. Clement, P. Suetens, Computerized craniofacial reconstruction: conceptual framework and review, Forensic Sci. Int. 201 (2010) 138–145, doi: http://dx.doi.org/10.1016/j.for- sciint.2010.03.008.

[17] A.F. Ridel, An Automated Computer-assisted Approximation of the Nose in South Africans from CBCT (Cone Beam Computed Tomography) Scans Doctoral dissertation, University of Pretoria, South Africa, 2018. http://hdl.handle.net/ 2263/71150.

[18] Munn, C.N. Stephan, Changes in face topography from supine-to-upright position—and soft tissue correction values for craniofacial identification, Forensic Sci. Int. 289 (2018) 40–50, doi: http://dx.doi.org/10.1016/j.for- sciint.2018.05.016.

[19] Fagertun, S. Harder, A. Rosengren, C. Moeller, T. Werge, R.R. Paulsen, T.F. Hansen, 3D facial landmarks: inter-operator variability of manual annotation, BMC Med. Imaging 14 (2014) 35, doi: http://dx.doi.org/10.1186/1471-2342-14- 35.

[20] A. Toma, A. Zhurov, R. Playle, E. Ong, S. Richmond, Reproducibility of facial soft tissue landmarks on 3D laser-scanned facial images, Orthod. Craniofac. Res. 12 (2009) 33–42. doi: http://dx.doi.org/10.1111/j.1601-6343.2008.01435.x.

[21] S.M. Weinberg, N.M. Scott, K. Neiswanger, C.A. Brandon, M.L. Marazita, Digital three-dimensional photogrammetry: evaluation of anthropometric precision and accuracy using a genex 3D camera system, Cleft Palate-craniofacial J. 41 (2004) 507–518. doi: http://dx.doi.org/10.1597/03-066.1.

[22] N. von Cramon-Taubadel, B.C. Frazier, M.M. Lahr, The problem of assessing landmark error in geometric morphometrics: theory, methods, and modifications, Am. J. Phys. Anthropol. 134 (2007) 24–35, doi: http://dx.doi.org/ 10.1002/ajpa.20616.

[23] Y. Wong, A.K. Oh, E. Ohta, A.T. Hunt, G.F. Rogers, J.B. Mulliken, C.K. Deutsch, Validity and reliability of craniofacial anthropometric measurement of 3D digital photogrammetric images, Cleft Palate-craniofacial J. 45 (2008) 232– 239. doi: http://dx.doi.org/10.1597/06-175.

[24] D. White, A. Ortega-Castrillón, H. Matthews, A.A. Zaidi, O. Ekrami, J. Snyders, Y. Fan, T. Penington, S. Van Dongen, M.D. Shriver, P. Claes, MeshMonk: Open-source large-scale

intensive 3D phenotyping, Sci. Rep. 9 (2019) 6085,
doi: http://dx.doi.org/10.1038/s41598-019-42533-y.L.

[25] G. Arnqvist, T. Mârtensson, Measurement error in geometric morphometrics: empirical strategies to assess and reduce its impact on measures of shape, Acta Zoologica Acaemiae Scientiarium Hungaricae 44 (1) (1998) 73–96.

[26] A. Pérez-Pérez, A. Alesan, L. Roca, Measurement error: inter-and intraobserver variability. An empiric study, Int. J. Anthropol. 5 (1990) 129–135.
doi: http://dx. doi.org/10.1007/BF02442082.

[27] S.M. Yezerinac, S.C. Lougheed, P. Handford, measurement error and morphometric studies: statistical power and observer experience, Syst. Biol. 41 (1992) 471–482.
doi: http://dx.doi.org/10.1093/sysbio/41.4.471.

[28] L.P. Menéndez, Comparing methods to assess intraobserver measurement error of 3D craniofacial landmarks using geometric morphometrics through a digitizer arm, J. Forensic Sci. 62 (2017) 741–746, doi: http://dx.doi.org/10.1111/ 1556-4029.13301.

[29] T.F. Cootes, C. Taylor, ”Active shape models search using grey level models: a quantitative evaluation”, Proceedings, British Machine Vision Conference (1993) 639–648 2.

[30] T.F. Cootes, G.J. Edwards, C.J. Taylor, Active appearance models, IEEE Trans. Pattern Anal. Mach. Intell. 23 (2001) 681–685, doi: http://dx.doi.org/10.1109/ 34.927467.

[31] Y. Wang, C.-S. Chua, Y.-K. Ho, Facial feature detection and face recognition from 2D and 3D images, Pattern Recognit. Lett. 23 (2002) 1191–1202.
doi: http://dx. doi.org/10.1016/S0167-8655(02)00066-1.

[32] D. Xi, S.-W. Lee, Face detection and facial component extraction by wavelet decomposition and support vector machines, Audio- and Video-Based Biometric Person Authentication, Springer, Berlin, Heidelberg, 2003, pp. 199–207.
doi: http://dx.doi.org/10.1007/3-540-44887-X_24.

[33] S. Kobayashi, S. Hashimoto, Automated feature extraction of face image and its applications, IEEE (1995) 164–169., doi: http://dx.doi.org/10.1109/RO- MAN.1995.531954.

[34] M.C. Ruiz, J. Illingworth, Automatic landmarking of faces in 3D-ALF, IEE (2008) 41–46, doi: http://dx.doi.org/10.1049/cp:20080280.

[35] W.C. Scarfe, A.G. Farman, What is cone-beam CT and how does it work? Dent. Clin. North Am. 52 (2008) 707–730, doi: http://dx.doi.org/10.1016/j. cden.2008.05.005.

[36] J.F. Hair, R.E. Anderson, R.L. Tatham, W.C. Black, Analisis Multivariante, Prentice-Hall, Madrid, Spain, 1999.

[37] C.F. Spoor, F.W. Zonneveld, G.A. Macho, Linear measurements of cortical bone and dental enamel by computed tomography: applications and problems, Am. J. Phys. Anthropol. 91 (1993) 469–484, doi: http://dx.doi.org/10.1002/ ajpa.1330910405.

[38] J. Caple, C.N. Stephan, A standardized nomenclature for craniofacial and facial anthropometry, Int. J. Legal Med. 130 (2016) 863–879.
doi: http://dx.doi.org/ 10.1007/s00414-015-1292-1.

[39] P. Claes, A Robust Statistical Surface Registration Framework Using Implicit Function Representations: Application in Craniofacial Reconstruction PhD Thesis, K.U. Leuven, Belgium, (2007).

[40] J. Snyders, P. Claes, D. Vandermeulen, P. Suetens, Development and Comparison of Non-rigid Surface Registration Algorithms and Extensions Technical report KUL/ESAT/PSI/1401, KU Leuven, ESAT, January, Leuven, Belgium, (2014).

[41] D.G. Kendall, Shape manifolds, procrustean metrics, and complex projective spaces, Bull. London Math. Soc. 16 (1984) 81–121, doi: http://dx.doi.org/ 10.1112/blms/16.2.81.

[42] D.E. Slice, Landmark coordinates aligned by Procrustes analysis do not lie in Kendall's shape space, Syst Biol. 50 (1) (2001) 141–149.

[43] F.L. Bookstein, Morphometric Tools for Landmark Data: Geometry and Biology, Cambridge University Press, Cambridge [England]; New York, 1991.

[44] F. Bookstein, Biometrics, biomathematics and the morphometric synthesis, Bull. Math. Biol. 58 (1996) 313–365, doi: http://dx.doi.org/10.1016/0092-8240 (95)00329-0.

[45] F.L. Bookstein, Shape and the information in medical images: a decade of the morphometric synthesis, IEEE (1996) 2–12.
doi: http://dx.doi.org/10.1109/ MMBIA.1996.534052.

[46] T.A. White, J.B. Searle, Mandible asymmetry and genetic diversity in island populations of the common shrew, Sorex araneus, J. Evol. Biol. 21 (2008) 636– 641, doi: http://dx.doi.org/10.1111/j.1420-9101.2007.01481.x.

[47] L.J. Leamy, C.P. Klingenberg, The Genetics and Evolution of Fluctuating Asymmetry, Annu. Rev. Ecol. Evol. Syst. 36 (2005) 1–21.
doi: http://dx.doi.org/ 10.1146/annurev.ecolsys.36.102003.152640.

[48] D.A. Schmieder, H.A. Benítez, I.M. Borissov, C. Fruciano, Bat species comparisons based on external morphology: a test of traditional versus geometric morphometric approaches, PLoS One 10 (2015)e0127043, doi: http://dx.doi.org/10.1371/journal.pone.0127043.

[49] C. Fruciano, Measurement error in geometric morphometrics, Dev. Genes Evol. 226 (3) (2016) 139–158.

[50] R Core Team, R: a Language and Environment for Statistical Computing, R Foundation for Statistical Computing, Vienna, Austria, 2012. http://www.R- project.org.

[51] Kyong I. Chang, K.W. Bowyer, P.J. Flynn, Multiplenose region matching for 3D face recognition under varying facial expression, IEEE Trans. Pattern Anal. Mach. Intell. 28 (2006) 1695–1700, doi: http://dx.doi.org/10.1109/TPAMI.2006.210.

[52] G. Zhang, Y. Wang, A 3D facial feature Point localization method based on statistical shape model, IEEE (2007) II-249–II-252.
doi: http://dx.doi.org/ 10.1109/ICASSP.2007.366219.

[53] M.P. Segundo, C. Queirolo, O.R.P. Bellon, L. Silva, Automatic 3D facial segmentation and landmark detection, IEEE (2007) 431–436.
doi: http://dx. doi.org/10.1109/ICIAP.2007.4362816.

[54] I.A. Kakadiaris, G. Passalis, G. Toderici, M.N. Murtuza, Y. Lu, N. Karampatziakis, T. Theoharis, Three-dimensional face recognition in the presence of facial expressions: an annotated deformable model approach, IEEE Trans. Pattern Anal. Mach. Intell. 29 (2007) 640–649, doi: http://dx.doi.org/10.1109/ TPAMI.2007.1017.

[55] Xiaoguang Lu, A.K. Jain, Automatic feature extraction for multiview 3D face recognition, IEEE (2006) 585–590., doi: http://dx.doi.org/10.1109/FGR.2006.23.